Single-charge effects in silicon nanocrystals probed by atomic force microscopy: From charge blinking to nanocrystal charging

Thierry Melin, D. Deresmes

Journal of Applied Physics

Single-charge effects in silicon nanocrystals probed by atomic force microscopy: From charge blinking to nanocrystal charging

Cite as: J. Appl. Phys. **130**, 065103 (2021); https://doi.org/10.1063/5.0054744
Submitted: 21 April 2021 • Accepted: 22 July 2021 • Published Online: 09 August 2021

Thierry Mélin and Dominique Deresmes

Journal of Applied Physics ARTICLE scitation.org/journal/jap

Single-charge effects in silicon nanocrystals probed by atomic force microscopy: From charge blinking to nanocrystal charging

Cite as: J. Appl. Phys. **130**, 065103 (2021); doi: 10.1063/5.0054744
Submitted: 21 April 2021 · Accepted: 22 July 2021 ·
Published Online: 9 August 2021

Thierry Mélin[a] and Dominique Deresmes

AFFILIATIONS

Univ. Lille, CNRS, Centrale Lille, Junia, Univ. Polytechnique Hauts-de-France, UMR 8520—IEMN, Institut d'Electronique de Microélectronique et de Nanotechnologie, F-59000 Lille, France

[a]**Author to whom correspondence should be addressed:** thierry.melin@iemn.fr

ABSTRACT

We investigate the electrical properties of individual silicon nanocrystals (NCs) by means of atomic/electrostatic force microscopy at atmospheric pressure, with the sensitivity of the elementary charge. Using a tip bias close to the sample surface potential for the sample topography imaging, NCs reveal charge blinking properties, corresponding to multi-state charge fluctuations of their defect states. A transition from the NC charge state blinking to NC charging is observed upon biasing the atomic force microscopy tip during topography imaging, leading to both charging of the sample oxide surface and of the NCs, together with faint diffusion of the NC charge along the sample oxide surface. Our results achieved with standard atomic force microscopy demonstrate the possibility to produce experimental results on the electrostatic properties of silicon nanocrystals in the elementary charge sensitivity limit, which is of primary importance for charge-sensitive electro-optical devices.

I. INTRODUCTION

Semiconductor nanocrystals (NCs) are important for their electronic properties, e.g., when used as inclusions in non-volatile memory devices[1] or for optical applications.[2] These two types of applications suggest the need for an ability to measure and understand the electrical charge states of individual nanocrystals. The application relevance is in assessing the capacity of NCs to store charges (as for charge retention device applications)[3] or the control of their defect states in the case of optical devices, which otherwise lead to charge fluctuations (trapping/detrapping) phenomena[4] and in turn generate fluorescence intermittency or optical blinking.[5] These physical issues have in common that they can be addressed at the scale of single NCs by means of scanning-probe microscopies and, in particular, via electrical modes derived from atomic force microscopy (AFM) such as electrostatic force microscopy (EFM) or Kelvin probe force microscopy. Hence, detailed work has been done so far to understand the charging properties of silicon NCs in view of memory applications.[3,6–11] A lot of work have also been performed on single charge fluctuations or blinking and, in particular, regarding the temporal statistics of these charge fluctuations. This has been achieved mostly using colloidal NCs and by means of optical techniques and also via electrical or scanning-probe techniques (see, for instance, Refs. 4, 5, and 12).

In this work, we make a link between these two electrical aspects of nanocrystals in the case of silicon NCs by means of electrostatic force microscopy. In particular, we observe *charge blinking* associated with individual silicon nanocrystals as well as the gradual transition between charge blinking and *nanocrystal charging*. Charge blinking is hence observed when the NCs are probed without external biasing, while electrical charging occurs as a result of capacitive charging as soon as a tip bias is applied while imaging the NCs during AFM topography. The entire work has been performed with an atomic force microscope operated at room temperature at atmospheric pressure, in the limit of the elementary charge sensitivity in the EFM mode. The article is organized as follows. In Sec. II, we describe the experimental EFM setup used to separate the charge effects from the capacitive effects and to obtain a single charge sensing sensitivity at atmospheric pressure. In Sec. III, we highlight the observed blinking phenomena at the scale of individual NCs, corresponding to multi-state fluctuations of their charge

state; we then study (Sec. IV) the transition between charge blinking and NC charging obtained by scanning the sample with a polarized AFM tip and identify (Sec. V) a faint diffusion of the NC charge along the sample oxide surface.

II. EXPERIMENTS

The samples used in this work are silicon nanocrystals synthesized by chemical vapor deposition on a 3 nm thick thermal silicon dioxide layer grown on a p-type silicon substrate with doping level of $\approx 10^{15}$ cm^{-3} and followed by the growth of a 1.2 nm thermal silicon dioxide.[13] Such a growth method leads to a NC surface density ranging from 10^{11} cm^{-2} up to a few 10^{11} cm^{-2} (depending on the growth nucleation time), mean heights ranging from a few nm to a few tens of nm, hemispherical NC shapes as observed from scanning-electron microscopy, and a monocrystalline structure as from high-resolution transmission electron microscopy images.[13] No further growth details are provided in this paper since the NCs correspond to the same NCs used in Ref. 7 for which a detailed description of the growth is provided in Ref. 13. All the work done in the present manuscript deals with the nanoscale electrical characterization of such NCs.

Experiments have been carried out with an atomic force microscope at atmospheric pressure (Nanoscope III, Bruker), operated under a flow of dry gaseous nitrogen to overcome surface oxidation processes during electrical experiments. The microscope is used for the sample topography in the tapping mode [see Fig. 1(a), a tip oscillation amplitude of $\simeq$30 nm, with tip bias V_t] and in the electrostatic force microscopy (EFM) mode using a $\omega/2\omega$ modulated scheme [see Fig. 1(b)]. This mode enhances the signal to noise ratio as compared to static EFM measurements. It has been used by Krauss and Brus[4] to characterize single charge fluctuations in colloidal CdSe nanocrystals. We used EFM-type nanosensor cantilevers (stiffness constant of a few N/m, a frequency of $\approx$75 kHz) with a PtIr metallization coating. The electrical EFM mode is "interleaved" with topography scan lines, and data are acquired in a linear (constant height) mode [see Fig. 1(b)] with a z-offset $z_{\text{lift}} = 50$ nm in order to avoid any short-range contact with the NCs during electrostatic measurements.

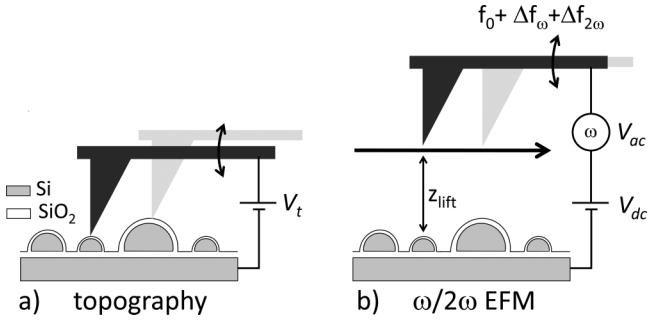

FIG. 1. (a) Schematics of the sample imaging in tapping mode. (b) Schematics of the electrical measurement in the linear (i.e., constant height) mode, in which the cantilever frequency shift (experimentally: phase shift) is mapped under the application of a dc + ac voltage to the tip. The tip is moved parallel to the substrate plane and lifted a distance z_{lift}. This separates charge effects (Δf_ω) and dielectric/capacitive effects ($\Delta f_{2\omega}$) at the angular frequencies ω and 2ω, respectively (see text).

To perform $\omega/2\omega$ EFM, a $V_{dc} + V_{ac}\cos(\omega t)$ voltage is applied to the tip at the angular frequency ω [sample at ground, see Fig. 1(b)]. V_{ac} is fixed at 4 V, while the static bias V_{dc} is chosen by the operator, and $\omega = 2\pi \times 510$ rad/s has been taken as a compromise between the scanning speed in the EFM mode and the microscope phase detector cut-off frequency of about 400 Hz (see hereafter). In a purely capacitive model, the application of the dc + ac voltage generates an electrostatic force gradient equal to $1/2\, d^2C/dz^2[V_{dc} - V_s + V_{ac}\cos(\omega t)]^2$, in which V_s is the sample surface potential, $C(z)$ the local tip-sample capacitance, and z is the tip-sample distance. This force gradient induces a cantilever oscillation frequency shift Δf.[14] Δf hence contains a component Δf_ω oscillating at the angular frequency ω, proportional to $d^2C/dz^2[V_{dc} - V_s]V_{ac}\cos(\omega t)$. It also contains a component $\Delta f_{2\omega}$ oscillating at the angular frequency 2ω, proportional to $d^2C/dz^2 V_{ac}^2\cos(2\omega t)$. In this capacitive model, Δf_ω can be set to zero by using $V_{dc} = V_s$ (this can be also used to measure local variations of V_s in a Kelvin mode), while $\Delta f_{2\omega}$ provides a purely "dielectric" measurement of the tip-sample capacitance via the variations of d^2C/dz^2 when scanning over the sample.

Assuming for simplicity that V_{dc} has been set to V_s on the sample oxide surface, a static sample charge Q carried, e.g., by a NC will then interact with the capacitive charge $C(z)V_{ac}\cos(\omega t)$ at the tip and lead to an additional cantilever frequency shift oscillating at the angular frequency ω. In this scheme, $\Delta f_{2\omega}$, therefore, provides a measurement of the tip-sample capacitance variations irrespective of the sample local charge Q, while Δf_ω enables the mapping of Q in a separate image. This has been illustrated in Ref. 4, in which the charge Q is the intermittent elementary charge carried by blinking colloidal NCs. In our work, the oxidized silicon substrate may also be sensitive to charging effect (for instance, by charging under the action of the topography imaging voltage V_t). The V_s component, therefore, may evolve with time as a result of occasional oxide charging: this effect, if relevant, will be observed via the time evolution of the Δf_ω image.

In practice, Δf_ω and $\Delta f_{2\omega}$ signals are obtained by the demodulation of the EFM cantilever oscillation phase, with an integration time constant τ of about $10 \times 2\pi/\omega$. This time constant limits the acquisition speed of the $\omega/2\omega$ EFM mode, given the bandwidth of the cantilever phase detector, here measured as about 400 Hz. ω has been taken here as $2\pi \times 510$ Hz ($\tau \approx 20$ ms), leading to coupled topography and $\omega/2\omega$ image acquisition lasting up to a few hours per image. The cantilever oscillation phase components at ω and 2ω (corresponding to Δf_ω and $\Delta f_{2\omega}$ signals) are externally demodulated using a lock-in amplifier and acquired as external signals on the atomic force microscope using an analog-to-digital converter with ± 10 V input range, in order to form the images of the sample charge and dielectric effects at the angular frequencies ω and 2ω, respectively.

III. NANOCRYSTAL SINGLE CHARGE AND BLINKING EFFECTS

The measurement method is first applied to the case of Si NCs for which the surface is probed with the tip at V_s during

topography imaging (choice of $V_{dc} = V_s$ on the sample oxide surface prior to imaging and use of $V_t = V_s$ during topography imaging).

We first proceed with a single Si NC with 20 nm height, for which the topography is shown in Fig. 2(a) (the 20 nm high NC appears here as fairly large as due to the tip-NC convolution) as well as two subsequent EFM maps in Figs. 2(b) and 2(c). Δf_ω and $\Delta f_{2\omega}$ (experimentally: demodulated cantilever phase shifts at ω and 2ω acquired via the AFM analog-to-digital converters) are, respectively, shown in Figs. 2(b_1) and 2(b_2) as well as Figs. 2(c_1) and 2(c_2). Each 128 × 128 pixel scan duration was about 45 min, and imaging was first obtained by scanning from top to bottom and then from bottom to top. The topography and $\Delta f_{2\omega}$ images are shown after a standard plane fit procedure. In the case of the $\Delta f_{2\omega}$ images, this corresponds to subtracting a global tip-surface capacitive effect, in order to show only the local increase of the tip-surface capacitance (or more precisely the increase of d^2C/dz^2) associated with the presence of the NC within the tip-substrate capacitance.[15] In the case of the Δf_ω images, no experimental treatment has been performed, and the continuous background measured on the oxide surface corresponds to the component proportional to $V_{ac}(V_{dc} - V_s)$, which has been nullified prior to imaging by biasing the tip at the surface potential V_s.

The two $\Delta f_{2\omega}$ images in Figs. 2(c_1) and 2(c_2) are similar and replicate the topography shown in Fig. 2(a), however with a lower resolution since only long-range electrostatic forces are probed here. The Δf_ω images in Figs. 2(b_1) and 2(b_2) show a signal, which is varying by steps while the tip scans the NC, corresponding to abrupt changes in the NC charge state. More precisely, in Fig. 2(b_1) (scanned from top to bottom), five jumps can be identified (labeled from A to E) corresponding to contrast transitions from moderate dark to a background gray contrast (A), then switching to a faintly bright contrast (B), then to the background gray contrast (C), followed by a switch to faintly bright contrast (D), and back to dark contrast (E). A similar behavior is observed during the subsequent scan in Fig. 2(b_2), with the occurrence of a pronounced dark contrast (between jumps E and D) and pronounced bright contrast (between jumps B and A). The two scans show that the switch in the NC charge state is triggered by the tip scanning over precise locations over the NC. The distance separation between the

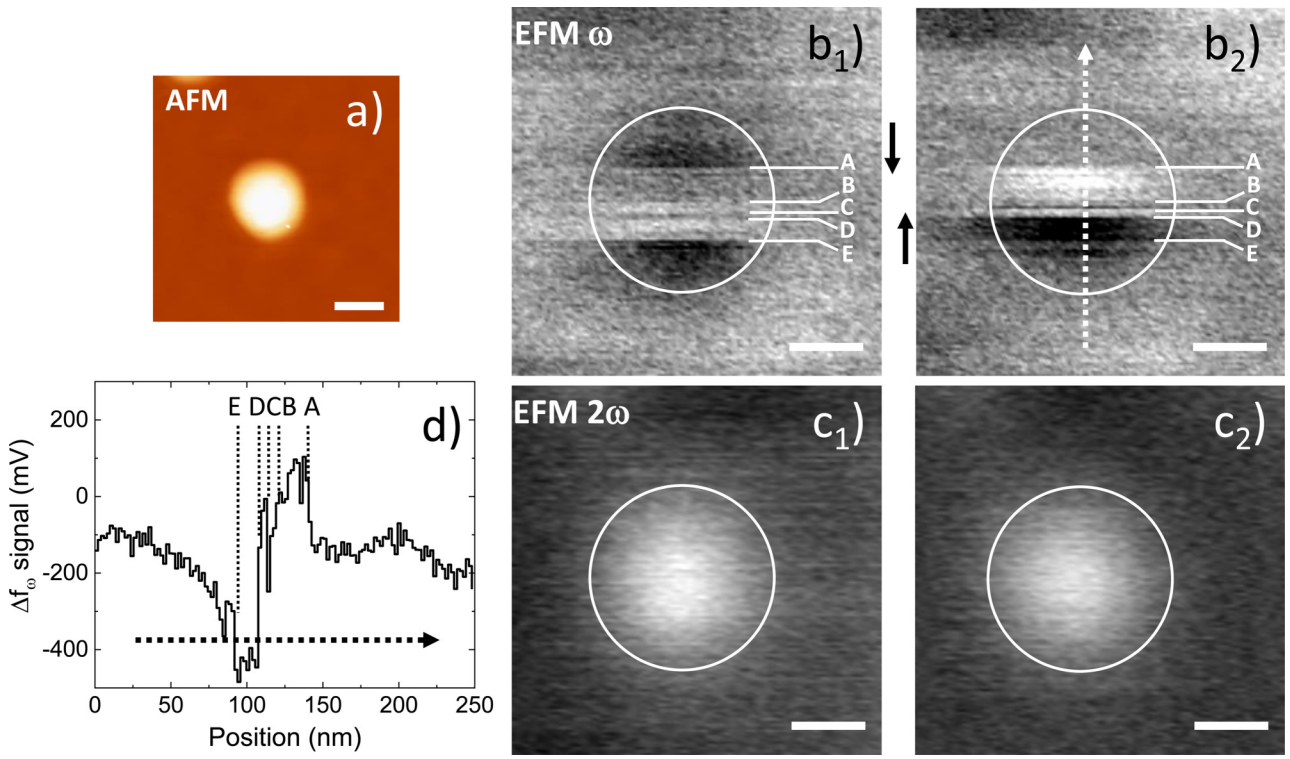

FIG. 2. (a) 250 × 250 nm^2 tapping-mode topography of a single NC with height 20 nm (128 × 128 pixel image). (b_1) and (b_2) Corresponding EFM images of the Δf_ω signal (see text) for two consecutively acquired scans. No image processing has been applied for these images. The short arrows account for the scanning directions. The gray scale range is 400 mV. The circles highlight the NC position as a guide to the eye. The events labeled from A to E correspond to changes in the NC charge state as the tip is scanned over the NC and correspond to elementary charge jumps (see text). The dotted arrow in (b_2) corresponds to the signal cross section shown in (d). (c_1) and (c_2) Simultaneously acquired EFM images of the $\Delta f_{2\omega}$ signal for two consecutively acquired scans. A plane fit procedure has here been used in order to remove the background tip-surface capacitance. The image gray scale range is 340 mV. (e) Cross section of the Δf_ω image shown in (b_2). The stepped signal corresponds to the Δf_ω128 × 128 image pixel size. The charge jumps A–E are identified. All scale bars in this figure are 50 nm.

charging events is only consistent with a charging process that is triggered during topography scanning. Since the charging also occurs at specific points on the NC surface, it is also likely related with surface or interface defect states (rather than NC volume charging), which are known to introduce hysteresis in the charging spectroscopy of NCs.[7] Only a few quantized charge states are identified, suggesting that we monitor here switching events with an elementary charge sensitivity, as observed in the pioneering work of Ref. 4 for single defect charging, with, however, here the NC charge belonging to an ensemble of five charge states $\{-2\Delta q, -\Delta q, 0, +\Delta q, +2\Delta q\}$. We reproduced in Fig. 2(d) a section (see arrow) of the Δf_ω signal of Fig. 2(c_1). Although the charging states are better observed directly as from Fig. 2(c_1), all transitions A–E can be identified on the cross section.

To demonstrate that the increment Δq corresponds to an elementary charge, we use previous work done on the quantitative measurement of NC charge states as from EFM signals, by computing the ratio $\mathcal{R}_\omega = \Delta f_\omega/\Delta f_{2\omega}$ between the charge and capacitive frequency (or phase) shifts.[15] We adapted the model to take into account the fact that we deal here with NC surface charges rather than a NC volume charge. The general idea of the analysis is to experimentally measure Δf_ω and $\Delta f_{2\omega}$ from Figs. 2(c) and 2(d). This yields a ratio $\mathcal{R}_\omega \approx 0.26$ for a charge jump Δq, from which we derive $\Delta q \approx 2$ e (see technical details in the following paragraph) for a model in which the main uncertainty comes from the NC base surface (an exact hemispherical shape has been assumed here). This order of magnitude supports the fact that the charging events observed in Fig. 2 are elementary charge jumps.

Technically, the analysis has been conducted as follows: we estimate from Fig. 2(d) the Δf_ω signal shift between the charge states $-2\Delta q$ and $+2\Delta q$ as ≈500 mV. Similarly, we obtain the capacitive phase shift from Figs. 2(c_1) or 2(c_2) as 225 mV, giving $\mathcal{R}_\omega$ = 0.55 for a single charge Δq. This ratio has to be corrected from the phase detector bandwidth cutoff of the atomic force microscope, which reduces values by a factor 0.54 for Δf_ω measured at $\omega = 2\pi \times 510$ rad/s, and by a factor 0.25 for the capacitive phase shift measured at 2ω. Thus, $\mathcal{R}_\omega \approx 0.26$, when corrected from bandwidth issues. From Ref. 15, $\mathcal{R}$ is expressed in the case of a volume charge as: $\mathcal{R}_\omega = \Delta f_\omega/\Delta f_{2\omega} = -2\frac{g}{\alpha}\frac{\Delta q/\epsilon}{\epsilon_0 S/zV_{ac}}$, in which $\alpha = 1.4$ accounts for the tip geometry, $g \approx 1$ is a prefactor accounting for the NC shape, S is the NC base surface, and z is the tip-substrate distance. In our case, the charge Δq is a point charge that is located at the NC surface, rather than a charge diluted in the NC volume; therefore, two effects take place: Δq generates an enhanced vertical dipole (enhancement factor 2 in a plane model) and the dielectric constant ϵ should be replaced $(1+\epsilon)/2$. By expressing Δq as a function of $\mathcal{R}_\omega$, one numerically finds $\Delta q \approx 2$e.

We now show in Fig. 3 a larger scale (500×500 nm^2) image showing five NCs. Three consecutive EFM scans are provided [Δf_ω in Fig. 3(b) and $\Delta f_{2\omega}$ in Fig. 3(c)] showing the time evolution of the NC charge state. Jumps in the NC charge state are evidenced for the five NCs, ranging from negative charging (dark features) to positive charging (bright features) in Figs. 3(b_1)–3(b_3). The smallest NC (for which no $\Delta f_{2\omega}$ signal is observed in the 2ω EFM image) showed similar behavior to the larger NCs. No time evolution trend is observed for the NC charge state, although the total

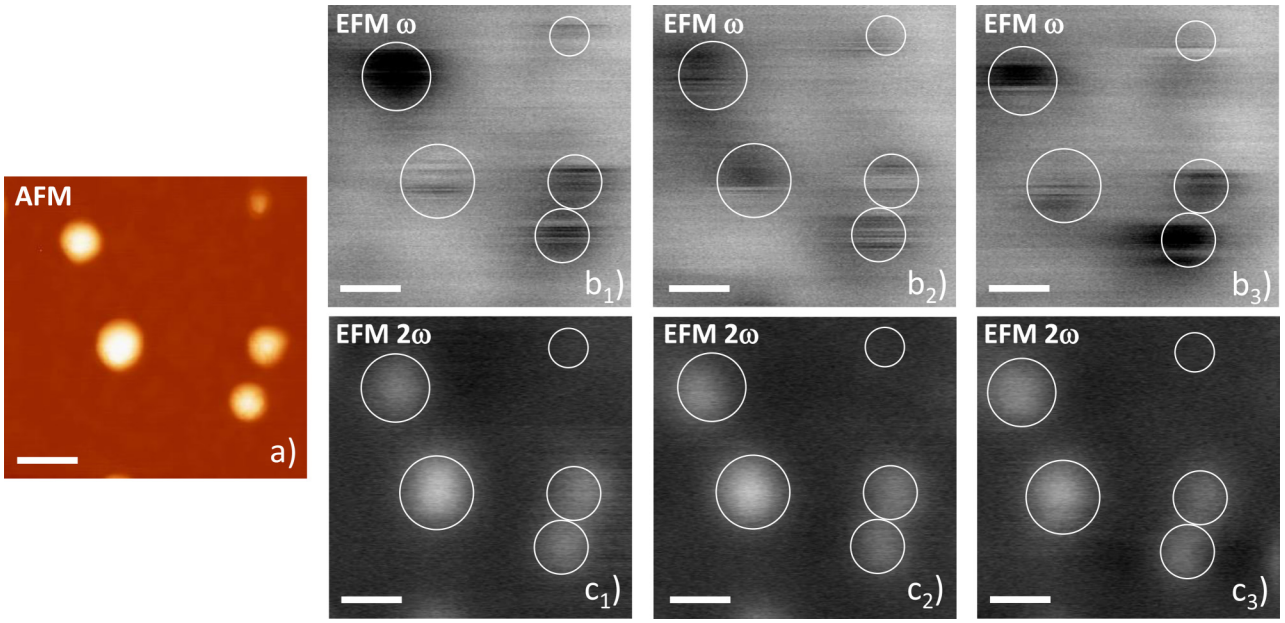

FIG. 3. (a) 500×500 nm^2 tapping-mode topography image showing five NCs (512×512 pixel image). (b_1)–(b_3) EFM images (6 h/frame) of the Δf_ω signal for three consecutive scans. No image processing has been applied for these images. The gray scale range is 1000 mV. The circles highlight the NC position as a guide to the eye. (c_1)–(c_3) Simultaneously acquired EFM images of the $\Delta f_{2\omega}$ signal for the three consecutive acquired scans. A plane fit procedure has been used to remove the background tip-surface capacitance. The image gray scale range is 450 mV. All scale bars in this figure are 100 nm.

duration of the three scans is here ≈18 h. This, therefore, links the NC charge jumps as a blinking behavior triggered by the electrical contact between the AFM tip and the NC surface, likely random charging surface defect states. The main difference here with the work of Ref. 4 lies in the observation of multiple possible charge states (Figs. 2 and 3), which may be related both to a larger number of NC defects as compared to colloidal NCs and/or defects exhibiting smaller charging energies (a charging energy of ≈200 meV has been estimated for CdSe NCs[12]).

IV. NANOCRYSTAL CHARGING VS BLINKING

We show now a set of experiments in which the tip bias V_t during topography scans is intentionally changed in order to induce charging effects. We show in Figs. 4(a_1) and 4(b_1) a $2 \times 1\,\mu m^2$ image of the sample surface (here only the topography in a_1 and Δf_ω image in b_1 images are represented), using $V_t = V_{dc} = 0.252$ V, after setting $V_{dc} = V_s = 0.252$ V by nullifying Δf_ω on the sample oxide surface. In the electrical image in Fig. 4(b_1), most NCs reveal a blinking behavior [see surrounded NCs in Figs. 4(a_1) and 4(b_1)] as already observed in Fig. 3, though the image is here obtained with a low 256 × 128 points resolution. We then switched the tip bias during topography to $V_t = -0.25$ V, while keeping V_{dc} unchanged during EFM detection. The corresponding AFM and EFM images recorded after ≈24h are shown in Figs. 4(a_2) and 4(b_2), respectively. A lateral drift is observed (corresponding to a drift below 10 nm/h), as evidenced by the set of NCs enhanced with dotted lines. Globally, the sample surface oxide shifts toward negative Δf_ω values of about −280 mV, which corresponds to a V_s surface potential shift of ≈−40 mV. The NC blinking appears suppressed in Fig. 4(b_2) as compared to Fig. 4(b_1), and most NCs exhibit a dark (or absent) contrast in the EFM image (see NCs highlighted with dotted lines), which attests to a NC negative charging. The same experiments have been repeated by switching the tip bias during topography to $V_t = +1.25$ V after the recording of Fig. 4(b) while keeping V_{dc} unchanged during EFM detection. The corresponding AFM and EFM images recorded after a continuous scanning during ≈60 h are shown in Figs. 4(a_3) and 4(b_3), respectively. The NCs then correspond to bright features in Fig. 4(b_3) (positive Δf_ω values) corresponding to a positive NC charging. Images in Fig. 4 show altogether that the blinking behavior observed when the tip is set at the surface potential [Fig. 4(b_1)] is replaced by a negative [Fig. 4(b_3)] or positive [Fig. 4(b_2)] NC charging.

V. NANOCRYSTAL GRADUAL CHARGING AND OXIDE CHARGE DIFFUSION

Figure 5 shows the gradual evolution of the sample electrical properties (i.e., surface and NC charging) upon tip biasing during topography imaging. To do so, we start from imaging conditions with $V_t = V_{dc} = V_s$ (measured as 0.18 V prior to the charging experiment). The tip bias during topography imaging is switched to $V_t = -1.2$ V, with V_{dc} left to 0.18 V at the beginning of a series of 15 successive large scale ($3 \times 3\,\mu m^2$) topography (color) and EFM (gray scale) images shown in Fig. 5(a). Only the Δf_ω images are shown in Fig. 5(a) since $\Delta f_{2\omega}$ do not evolve with time. The same gray scale range is used in all images, showing a gradual negative charging of the SiO_2 background as well as the NC charging and apparent coalescence of the NC charge pattern, as from Fig. 5(a). A set of three zoomed EFM images is shown in Fig. 5(b), corresponding to highlighted zones in Δf_ω images in Fig. 5(a). The first image shows NCs with systematic faintly bright to dark transitions as soon as the AFM tip passes over the NC top, which evidences abrupt negative charging upon scanning the NCs with the biased tip. The same abrupt charging events are observed in

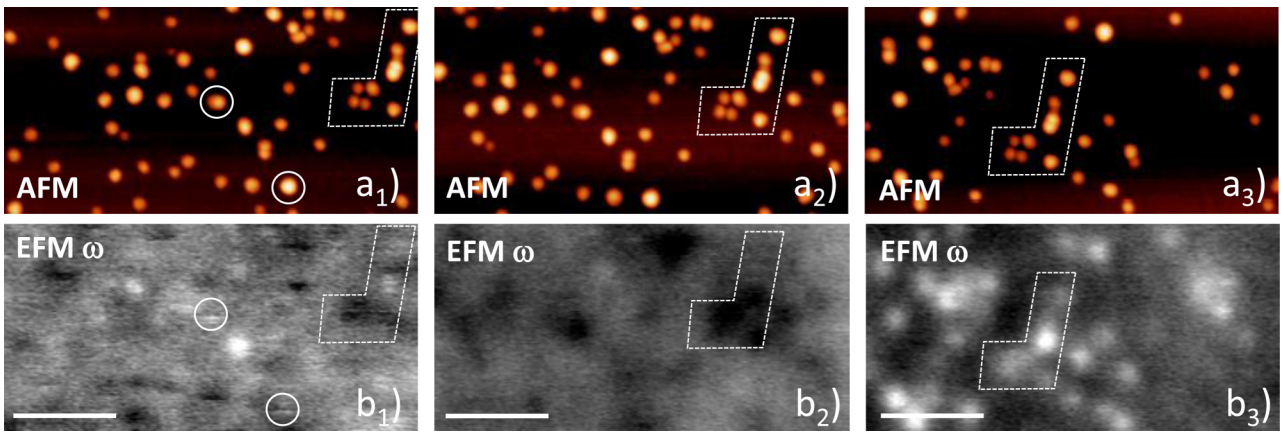

FIG. 4. (a_1)–(a_3) $2 \times 1\,\mu m^2$ tapping-mode topography images, with (b_1)–(b_3) being the corresponding Δf_ω EFM images ($\Delta f_{2\omega}$ images are not represented here). The tip has been initially biased with $V_t = V_{dc} = V_s = 0.252$ V in (a_1) and (b_1), and V_t set to −0.25 V (V_{dc} unchanged) afterward. (a_2) and (b_2) have been recorded ≈24 h after (a_1) and (b_1). V_t has been set to +1.25 V (V_{dc} unchanged) after (a_2) and (b_2). The images in (a_3) and (b_3) have been recorded ≈60 h after (a_2) and (b_2). EFM image gray scales are 670 mV in (b_1), and 1100 mV in (b_2) and (b_3), using a background offset so as to keep a similar gray background for the sake of clarity. The surrounded NCs are shown as a guide to the eye (see text). The dotted polygon is shown for the sake of clarity to indicate the drift between the three images (see text). All scale bars in this figure are 400 nm.

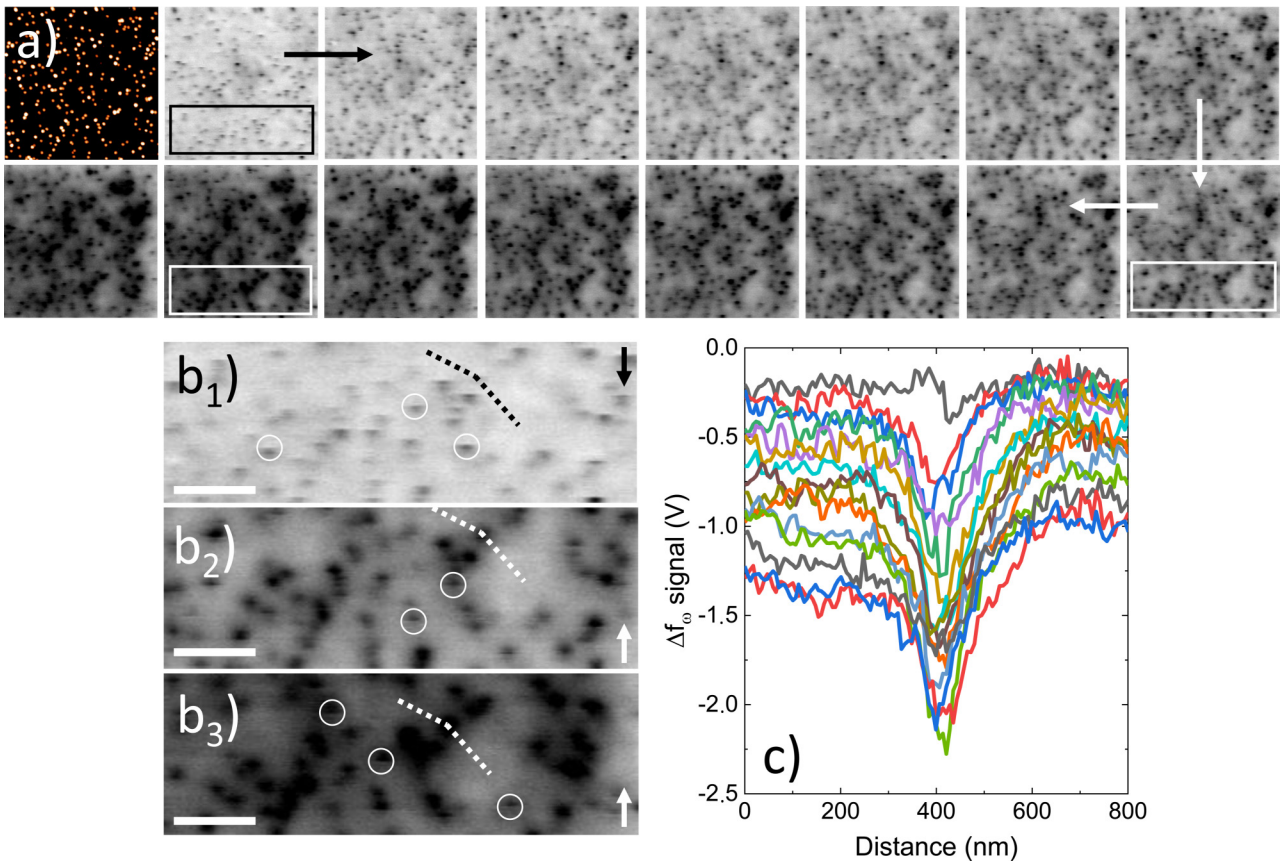

FIG. 5. (a) $3 \times 3\,\mu m^2$ atomic force microscopy scanand corresponding 15 successive EFM scans (gray scale), only showing here Δf_ω data. The tip has been switched from $V_t = V_{dc} = V_s = 0.18$ V to $V_t = -1.2$ V (with V_{dc} left to 0.18 V) at the start of the first scan. Each scan duration is about 5 h and 30 min, leading to some drift over the full imaging sequence. All EFM scans are raw data shown with the same color in the range of 1940 mV. (b_1)–(b_3) Zoomed scans corresponding to the three highlighted areas in (a). The arrows indicate the scanning direction (from top to bottom or bottom to top). The scale bars are 500 nm. The circled NCs in (b_1)–(b_3) highlight abrupt NC charging mechanisms. The kinked dotted lines correspond to the cross section used to plot EFM profiles in (c) across an isolated NC together with a well-defined signal reference on the SiO_2 substrate. It also enables us to visualize the drift between the three zoomed scans. (c) Δf_ω cross sections across the isolated NC shown in (b). The cross sections have been plotted for all EFM scans shown in (a), using an automatic software drift compensation procedure (see text).

subsequent images, with charging events correlated to the scan direction (i.e., from top to bottom or bottom to top). The NC and surface charging are further analyzed by performing signal cross sections across an isolated NC. The NC and the cross-section profile have been selected in order to obtain a clear reference for EFM data on the silicon substrate. The (kinked) cross-section profile is indicated in Figs. 5(b_1)–5(b_3) by white dotted lines and extends over ≈800 nm. The three scans in Figs. 5(b_1)–5(b_3) together with the cross sections show, in particular, the importance of drift due to the long AFM acquisition times during the 15 scans shown in Fig. 5(a). Cross sections across a single NC have, therefore, been plotted in Fig. 5(c), after using a drift calibration procedure between the 15 scans shown in Fig. 5(a).[16] The colors of the cross sections have not been labeled for the sake of clarity but the time evolution of both the SiO_2 background EFM signal and the NC EFM signal will later be analyzed and plotted as a function of the scan number (i.e., as a function of time). The plot in Fig. 5(c), hence, shows the raw EFM data of both SiO_2 and NC charging dynamics.

To perform a deeper analysis, we first analyze the SiO_2 surface Δf_ω charging signal, as plotted in Fig. 6(a), showing a linear evolution as a function of the scan number. For this analysis, the Δf_ω signal recorded on the AFM analog-to-digital converter can be converted into a shift ΔV_s of the sample surface potential, as indicated by the ΔV_s scale bar in Fig. 6(a). The oxide charging corresponds to a change in V_s, which stays lower than ≈200 mV, in spite of the applied change in V_t of the order of ≃1.4 V. This altogether means that a charging equilibrium of the SiO_2 surface has not been reached, although the total continuous scanning duration of the experiment is of about 3.5 days. This dynamics is relatively long with respect to the charging dynamics observed by contact-mode charging as in Ref. 7. This can be explained by the longer contact

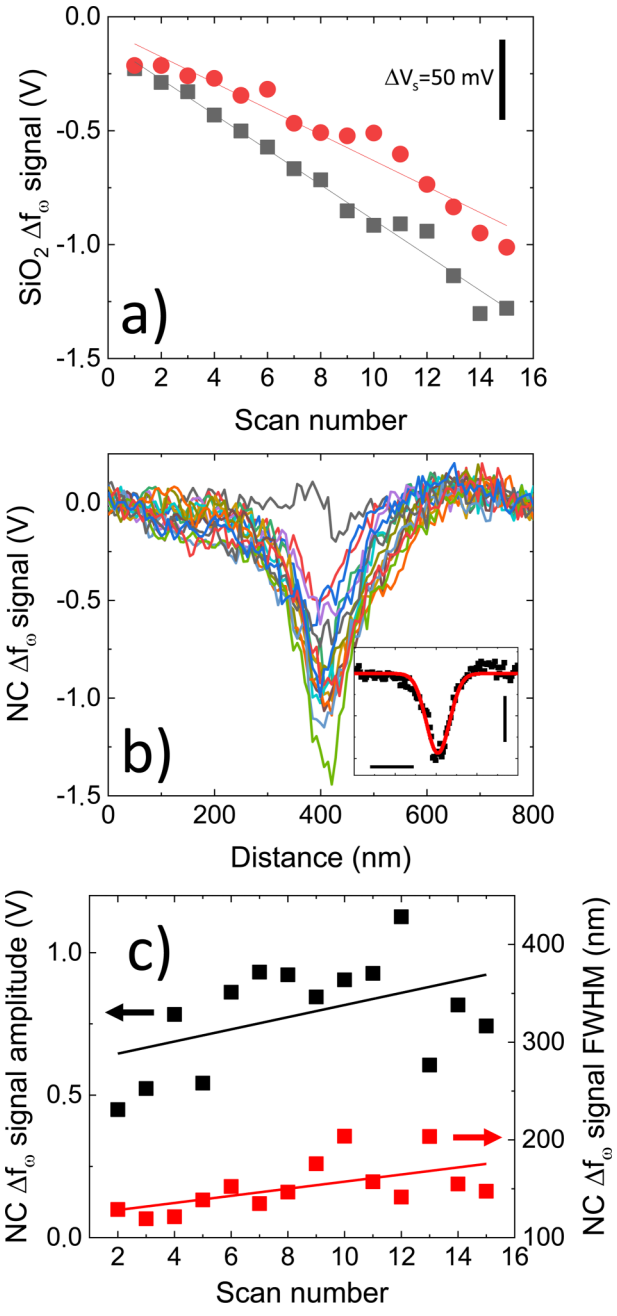

FIG. 6. (a) Evolution of the background SiO_2 charging Δf_ω signal both taken on the left and right hand sides of the NC cross sections in Fig. 5(c). Data have been plotted as a function of the number of the scan within the scan series shown in Fig. 5(a). The lines are linear fits to experimental data, as a guide to the eye. The ΔV_s vertical scale bar indicates the correspondence between the recorded Δf_ω signal and V_s. (b) NC charging signal Δf_ω after subtraction of the SiO_2 charging contribution. The inset illustrates a gaussian fit (red solid line) to a given experimental cross section (the scale bars are 200 nm and 0.5 V). (c) Fitted gaussian parameters (peak amplitude and FWHM) plotted as a function of the scan number.

time in contact-mode charging as compared to tapping-mode charging used in our present work.

We finally focus on the NC EFM signal itself. For this purpose, we corrected the experimental Δf_ω signal shown in Fig. 5(c) from the oxide charging background signal. The corresponding NC Δf_ω signal cross sections are shown in Fig. 6(b). In order to analyze the NC Δf_ω signal amplitude and full width at half maximum (FWHM), we use gaussian fits to experimental data [see example in Fig. 6(b), inset, in which the red solid line is a gaussian fit to experimental data points]. We then reported in Fig. 6(c) the time evolution of NC Δf_ω signal peak value (black points) and FWHM values (red points). The linear increase of the NC Δf_ω signal peak value [black points in Fig. 6(c)] is consistent with the linear increase of the oxide charging observed in Fig. 6(a), while the faint but observable increase of the Δf_ω FWHM values [red points in Fig. 6(c)] demonstrates the existence of a charge diffusion process from the NC to its environment. This likely occurs via the NC oxide surface since the NC charge signal shape should not depend on the charge value for charges stored in the NC volume.[17] The observation of a surface charge diffusion is consistent with the hysteretic behavior previously observed in the charge–voltage characteristics of NCs.[7]

A diffusion model can be tentatively applied to the fitted linear behavior of the FWHM parameter in Fig. 6(c), in which the increase in FWHM is due to the charge diffusion with characteristics length Dt at time t. This gives the following equation: $W^2 = W_0^2 + 16\ln(2)Dt$, in which W is the gaussian FWHM and D is the charge diffusion coefficient. A linearization provides the increase rate for W: $8\ln(2)D/W_0$. Using a fitted linear increase rate of 3.64 nm/scan as from Fig. 6(c), we find an estimation for $D \approx 2 \times 10^{-7}\ \mu m^2\ min^{-1}$. This value is most likely underestimated since the NC Δf_ω charge signal (on which gaussian fits are achieved) contains both information about the NC volume charge and oxide charge (while only the oxide charge diffuses). Little information, however, exists about the measurement of two-dimensional charge diffusion coefficients. Higher temperature experiments have been performed by He *et al.* in a one-dimensional geometry, using the channel of a carbon nanotube field effect transistor as a charge injection electrode into an oxide layer,[18] and measuring the injected charge diffusion coefficient with respect to temperature. By extrapolating the charge diffusion coefficient in the absence of water down to room temperature as from Ref. 18, we find $D \approx 5 \times 10^{-4}\ \mu m^2\ min^{-1}$. The difference in the two diffusion coefficient values may—in addition to the estimation or extrapolation uncertainties—stem from the difference in oxide layer thicknesses in both configurations since our experiments here deal with ultrathin tunnel oxides.

VI. CONCLUSION

We have in this work investigated the electrical properties of individual NCs using electrostatic force microscopy at atmospheric pressure with an elementary charge sensitivity. NCs reveal charge blinking properties when imaged with the microscope tip at the sample surface potential due to multi-state charge fluctuations of their defect states. This contrasts with the case of colloidal NCs, for which only single defect charging is observed. We observed a transition from charge blinking to NC charging as soon as the atomic

force microscopy tip bias is offset with respect to the sample surface potential during topography imaging, leading both to a gradual charging of the sample oxide surface and of the NCs. A relatively faint diffusion with the NC charge along the sample oxide surface is observed, enabling an estimation of their diffusion coefficient. This work underlines the possibility to reach ultimate and complex characterizations of nanostructures using standard atomic force microscopy, i.e., close to operating conditions for realistic nanodevices. This can help us in the understanding nanoscale electrical devices operating at the single charge level, which are sensitive to their local environment. This also holds for optical devices for which single charged nanostructures (such as blinking nanocrystals) may require a detailed characterization at the nanoscale.

ACKNOWLEDGMENTS

This work has been carried out using the facilities of the RENATECH network. We thank T. Baron (LTM-CNRS) for having provided us with the NC samples and T. Lerond for careful reading of the manuscript.

DATA AVAILABILITY

The data that support the findings of this study are available from the corresponding author upon reasonable request.

REFERENCES

[1]*Nanocrystals in Nonvolatile Memory*, edited by W. Banerjee (Pan Stanford Publishing, Singapore, 2018).
[2]*Nanocrystals Quantum Dots*, edited by V. I. Klimov (CRC Press, Boca Raton, 2010).
[3]E. Boer, L. Bell, M. Brongersma, H. Atwater, M. Ostraat, and R. Flagan, "Charging of single Si nanocrystals by atomic force microscopy," Appl. Phys. Lett. **78**, 3133 (2001).
[4]T. Krauss and L. Brus, "Charge, polarizability, and photoionization of single semiconductor nanocrystals," Phys. Rev. Lett. **83**, 359 (1999).
[5]C. Galland, Y. Ghosh, A. Steinbruck, M. Sykora, J. Hollingsworth, V. Klimov, and H. Htoon, "Two types of luminescence blinking revealed by spectroelectrochemistry of single quantum dots," Nature **479**, 203 (2011).
[6]T. Mélin, D. Deresmes, and D. Stiévenard, "Charge injection in individual silicon nanoparticles deposited on a conductive substrate," Appl. Phys. Lett. **81**, 5054 (2002).
[7]H. Diesinger, T. Mélin, D. Deresmes, and D. Stiévenard, "Hysteretic behavior of the charge injection in single silicon nanoparticles," Appl. Phys. Lett. **85**, 3546 (2004).
[8]M. J. Gordon and T. Baron, "Amplitude-mode electrostatic force microscopy in UHV: Quantification of nanocrystal charge storage," Phys. Rev. B **72**, 165420 (2005).
[9]G. M. Tao Feng and H. A. Atwater, "Charge retention characteristics of silicon nanocrystal layers by ultrahigh vacuum atomic force microscopy," J. Appl. Phys. **102**, 034305 (2004).
[10]A. Liscio, V. Palermo, and P. Samorì, "Nanoscale quantitative measurement of the potential of charged nanostructures by electrostatic and Kelvin probe force microscopy: Unraveling electronic processes in complex materials," Acc. Chem. Res. **43**, 541–550 (2010).
[11]F. Fuchs, F. Caffy, R. Demadrille, T. Mélin, and B. Grévin, "High-resolution Kelvin probe force microscopy imaging of interface dipoles and photogenerated charges in organic donor–acceptor photovoltaic blends," ACS Nano **10**, 739–746 (2016).
[12]E. Zbydniewska, A. Duzynska, M. Popoff, D. Hourlier, S. Lenfant, J. Judek, M. Zdrojek, and T. Mélin, "Charge blinking statistics of semiconductor nanocrystals revealed by carbon nanotube single charge sensors," Nano Lett. **15**, 6349 (2015).
[13]F. Mazen, T. Baron, A. Papon, R. Truche, and J. Hartmann, "A two steps CVD process for the growth of silicon nano-crystals," Appl. Surf. Sci. **214**, 4840 (2003).
[14]The cantilever frequency shift Δf is detected experimentally via the cantilever oscillation phase shift while exciting the cantilever at a fixed frequency. Since both quantities are proportional in the small frequency shift limit, we only refer in the manuscript to the cantilever resonance frequency shift Δf, although experiments are in practice based on the cantilever phase shifts.
[15]T. Mélin, H. Diesinger, D. Deresmes, and D. Stiévenard, "Electric force microscopy of individually charged nanoparticles on conductors: An analytical model for quantitative charge imaging," Phys. Rev. B **69**, 035321 (2004).
[16]I. Horcas, R. Fernández, J. Gomez-Rodriguez, J. Colchero, J. Gomez-Herrero, and A. Baror, "WSXM: A software for scanning probe microscopy and a tool for nanotechnology," Rev. Sci. Instrum. **78**, 013705 (2007).
[17]T. Mélin, H. Diesinger, D. Deresmes, and D. Stiévenard, "Probing nanoscale dipole–dipole interactions by electric force microscopy," Phys. Rev. Lett. **92**, 166101 (2004).
[18]Y. He, H. G. Ong, Y. Zhao, S. He, L.-J. Li, and J. Wang, "Study of charge diffusion at the carbon nanotube–SiO_2 interface by electrostatic force microscopy," J. Phys. Chem. C **113**, 15476–15479 (2009).